materials, and at low temperatures, the bolt shaft shrinks less than the washers and plates together. The contact pressure applied at room temperature is released and the thermal contact resistance between joint components increases significantly. For higher temperature levels, this effect is inverse. The fact that only one curve fits the experimental points obtained from different mounting configurations, shows that the parameter temperature, for low temperature levels, affects the overall thermal resistance more than any other parameter.

On the other side, from mean to high temperature levels (temperatures between -70 and $+40$°C), the overall thermal resistances present a large range of variation for similar joints (see second plot of Fig. 2). The thermal resistances are expected to increase with the increase in the number of washers since, for each washer inserted in the junction, two new thermal contact resistances (between washers) appear. Even if this trend can be observed, this effect is not clear. Actually, the experimental points are spread around the mean curve. This happens because most of the stainless steel washers are not perfectly flat and some contacts between washers may not occur over the entire area. Therefore, a constriction resistance in the radial direction of the washer may appear (see Fig. 1). Since the washer is thin and its material has a low thermal conductivity, this constriction resistance may be large.

In the third plot of Fig. 2, a comparison among the thermal resistance of mountings made of aluminum washers, mountings made of fiberglass and epoxy washers, and the overall mean thermal resistance curve is presented. Considering the thermal conductivity of the aluminum, which is the largest among other washers tested, the thermal resistance points for the aluminum washer mountings are expected to be under the overall thermal resistance curve. In addition, the fabrication process, special for the aluminum washers (they could not be found in the market), resulted in washers with low surface deformation. In opposition, the surfaces of the aluminum washer surfaces are rougher than those of SS washers, increasing the overall thermal resistance. The position of the experimental points under the mean curve demonstrates that, for these mountings, the material resistance decreases in a higher rate than the contact resistance increases.

The fiberglass and epoxy washers have the lowest thermal conductivity of all the washers used. Therefore, the overall thermal resistance is expected to be above the mean curve. This effect is observed only for high-temperature levels. The physical properties of this material change very much with the temperature, vacuum, and torque conditions, and the combination of these effects leads to an unpredictable behavior. Therefore, fiberglass and epoxy washers are not recommended for use in space applications.

All of the points for mountings assembled with titanium bolts are located under the mean curve. Also, for these mountings, the overall thermal resistance presents a small variation with the temperature level. This effect is expected, since the coefficient of thermal expansion of the titanium is lower than that of the SS, and therefore, the temperature has a lower effect in the overall thermal resistance. Finally, the overall thermal resistance, as well as its range of variation, decrease with the increase in the applied torque, as expected (see Fig. 2).

Conclusions

The temperature level is the controlling factor for temperatures less than -70°C. The combination of the coefficients of thermal expansion of the materials of the bolted joint components leads to this effect.

For mean to high-temperature levels (-70 to $+40$°C), the number of washers is not a controlling parameter if the washers present deformation resultant from the fabrication process. The material of the washers has a great influence in the overall thermal resistance. The fiberglass and epoxy washers are not recommended for satellite applications.

The range of variation of the thermal resistance is large, sometimes of the same order of magnitude of the values as the overall thermal resistances. The satellite-mounting procedures adopted resulted in bolted joints whose thermal resistances are difficult to estimate with precision. Therefore, the uncertainty in the estimation of the thermal resistance of bolted joints is high and large coefficients of safety must be used for the thermal design of satellites. Finally, the use of these bolted joints as satellite thermal control devices is not recommended.

Acknowledgments

M. B. H. Mantelli acknowledges the support of INPE and the financial support from CNPq, Grant 202018/91.1.

References

[1]Aron, W., and Colombo, G., "Controlling Factors of Thermal Resistance Across Bolted Joints in a Vacuum Environment," American Society of Mechanical Engineers Paper 63-WA-196, Aug. 1963.

[2]Eliott, D. H., "Thermal Conduction Across Aluminum Bolted Joints," American Society of Mechanical Engineers Paper 65-HT-53, May 1965.

[3]Fletcher, L. S., Peterson, G. P., Madhusudana, C. V., and Groll, E., "Constriction Resistance Through Bolted and Riveted Joints," *Journal of Heat Transfer*, Vol. 112, Nov. 1990, pp. 857–863.

[4]Song, S., Moran, K. P., Augi, R., and Lee, S. "Experimental Study and Modelling of Thermal Contact Resistance Across Bolted Joints," AIAA Paper 93-0844, Jan. 1991.

[5]Moffat, R. J., "Describing the Uncertainties in Experimental Results," *Experimental Thermal and Fluid Science*, Vol. 1, 1988, pp. 3–17.

[6]Kline, S. J., and McClintock, F. A., "Describing the Uncertainties in Simple-Sample Experiments," *Mechanical Engineering*, Jan. 1953, pp. 3–8.

Optimization Analysis of a Disk-Shaped Heat Pipe

N. Zhu* and K. Vafai†
Ohio State University, Columbus, Ohio 43210

Nomenclature

h	=	thickness, m
K	=	permeability of wicks, m^2
p	=	pressure, Pa
u, v, w	=	radial, vertical, angular velocity components, m/s
ε	=	porosity of wicks
μ	=	dynamic viscosity, N·s/m^2
ρ	=	density, kg/m^3
Φ	=	angle of each internal flow channel of the disk-shaped heat pipe

Subscripts

l	=	liquid phase
v	=	vapor phase

Received Jan. 3, 1995; revision received Aug. 3, 1995; accepted for publication Aug. 3, 1995.

*Research Assistant, Department of Mechanical Engineering.
†Professor, Department of Mechanical Engineering. Member AIAA.

vw = vertical wick
w = top and bottom wicks

Superscripts
b = bottom wick
t = top wick

Introduction

BECAUSE of the simplicity of conventional cylindrical heat pipes the influence of the heat pipe design parameters on the heat pipe performance has received little attention. For the asymmetrical disk-shaped heat pipe proposed by Vafai et al.,[1] however, the flow and heat transfer is significantly more complicated and the optimization of the heat pipe design is more prominent. Zhu and Vafai[2] have developed an analytical model for the vapor and liquid flow in the disk-shaped heat pipe that accounts for the liquid flow in the vertical wicks, the different liquid flow rates in the top and bottom wicks, the hydrodynamic coupling of the vapor and liquid phases, and the effects of non-Darcian transport. In the present study, this model is incorporated to predict the performance and to study the influence of the design parameters on the performance of the disk-shaped heat pipe. The criteria of capillary and boiling limitations are established for the asymmetrical disk-shaped heat pipe. The maximum heat transfer capacity of the disk-shaped heat pipe is predicted based on the analysis of the capillary limitation. The influence of the number of internal channels, the thickness and shape parameter of the top and bottom wicks, as well as the thickness and shape parameter of vertical wicks on the heat pipe performance is investigated. An optimized disk-shaped heat pipe design is obtained based on the parametric study and the analysis of the boiling limitation.

Formulation and Analysis

The description and schematic diagram of the disk-shaped heat pipe is given in Zhu and Vafai.[2] In the present analysis, vapor and liquid flows are assumed to be steady, laminar, and incompressible. In addition, the transport properties of the vapor and liquid are assumed to be constant along the heat pipe. All wicks are assumed isotropic and saturated with wetting liquid. Based on physical considerations, the vapor injection and suction rates are taken as uniform on the top and bottom wicks and negligible on the vertical wicks. Therefore, the vapor velocity component in the θ direction is negligible.

Vapor Flow Dynamics

Based on the previous assumptions, the continuity Eq. (1) and the r-momentum Eq. (2) govern the vapor flow

$$\frac{\partial u_v}{\partial r} + \frac{\partial v_v}{\partial y} + \frac{u_v}{r} = 0 \tag{1}$$

$$\rho_v\left(u_v\frac{\partial u_v}{\partial r} + v_v\frac{\partial u_v}{\partial y}\right) = -\frac{\partial p_v}{\partial r} + \mu_v\left(\frac{\partial^2 u_v}{\partial r^2} + \frac{1}{r}\frac{\partial u_v}{\partial r} - \frac{u_v}{r^2} + \frac{\partial^2 u_v}{\partial y^2} + \frac{1}{r^2}\frac{\partial^2 u_v}{\partial \theta^2}\right) \tag{2}$$

Liquid Flow in the Wicks

The governing equations for the liquid flow in the top and bottom wicks are

$$\frac{1}{r}\frac{\partial}{\partial r}(ru_l^i) + \frac{\partial v_l^i}{\partial y} + \frac{1}{r}\frac{\partial w_l^i}{\partial \theta} = 0 \tag{3}$$

$$\frac{\mu_l}{\varepsilon_w}\left(\frac{\partial^2 u_l^i}{\partial r^2} + \frac{1}{r}\frac{\partial u_l^i}{\partial r} - \frac{u_l^i}{r^2} + \frac{\partial^2 u_l^i}{\partial y^2} + \frac{1}{r^2}\frac{\partial^2 u_l^i}{\partial \theta^2}\right) - \frac{\mu_l}{K_w}u_l^i - \frac{\rho_l F\varepsilon_w}{K_w^{1/2}}|u_l^i|u_l^i - \frac{\partial p_l^i}{\partial r} = 0 \tag{4}$$

$$i = \begin{cases} t & \text{for top liquid-wick region} \\ b & \text{for bottom liquid-wick region} \end{cases}$$

The geometric function F is calculated using the expression outlined in Vafai.[3] The mass conservation for the liquid within the vertical wicks yields

$$Q(r) = \int_{-h_w}^{0}[w_l^b(r, y, \theta = \Phi) - w_l^b(r, y, \theta = 0)]\,dy = -\int_{h_v}^{h_v+h_w}[w_l^t(r, y, \theta = \Phi) - w_l^t(r, y, \theta = 0)]\,dy \tag{5}$$

For the horizontal heat pipe under study, the liquid flow within the vertical wicks is based on Darcy's law:

$$Q(r) = -\frac{K_{vw}h_{vw}}{\mu_l}\left[\frac{p_l^t(r) - p_l^b(r)}{h_v} + \rho_l g\right] \tag{6}$$

Maximum Heat Transport Capillary Limit

Based on the analysis given by Zhu and Vafai,[2] the maximum heat transfer attainable in the heat pipe is achieved when the sum of the pressure losses along the vapor–liquid path for the top wall is equal to the maximum possible capillary pressure, i.e.,

$$\frac{2\sigma_l}{r_{c,w}} = \Delta p_v^t(r_{\max} - R) + \Delta p_l^t(R - r_{\max}) + p_c^t(R) \tag{7}$$

where $p_c(R) = p_v(R) - p_l(R)$, $r_{c,w}$ is the effective pore radius of the top and bottom wicks, σ_l is the surface tension of the working liquid in the wick, and $r_{\max}$ denotes the location where the capillary pressure is maximum. The notation $\Delta p(r_{\max} - R)$ means that Δp is evaluated over the distance $(r_{\max} - R)$.

Maximum Heat Transport Boiling Limit

Based on the analysis given in Chi,[4] and noticing that the heat pipe wick is flat, the following expression is derived for the boiling limit of the disk-shaped heat pipe:

$$q_{b,\max} = \frac{k_w T_v}{\rho_v h_{fg} h_w}\left(\frac{2\sigma_l}{r_n} - \frac{2\sigma_l}{r_{c,w}}\right) \tag{8}$$

where T_v is the vapor temperature, h_{fg} is the latent heat of the working fluid, k_w is the effective thermal conductivity of the liquid-saturated wick, and r_n is the nucleation radius of the vapor bubbles.

The vapor–liquid hydrodynamic coupling conditions at the vapor–liquid interfaces and the boundary conditions are given in Zhu and Vafai.[2] An in-depth integral analysis along with the method of matched asymptotic expansions is employed to obtain the ordinary differential equations (ODEs) for vapor and liquid velocity and pressure distributions. The detail of the analysis is presented in Zhu and Vafai.[2] The fourth-order Runge–Kutta method is used to solve these ODEs and the maximum heat transfer capacity of the disk-shaped heat pipe is obtained iteratively.

Results and Discussion

The results are based on a disk-shaped heat pipe with heavy water as the working fluid. To analyze and optimize the effects

of various parameters a baseline set of parameters are chosen based on some practical considerations. The radius of the copper heat pipe R is taken as 0.25 m and the thickness of the heat pipe $H = h_v + 2h_w$, is taken as 0.03 m. The radius of the circular heat input zone is 0.125 m. Φ is chosen as 45 deg. The top, bottom, and vertical wicks are sintered copper powder with baseline parameters taken as $h_w = h_{vw} = 0.003$ m, $r_{c,w} = 35.8\ \mu$m, $\varepsilon_w = 0.61$, $K_w = 4.25 \times 10^{-11}$ m^2, $r_{c,vw} = 9\ \mu$m, $\varepsilon_{vw} = 0.52$, and $K_{vw} = 1.74 \times 10^{-12}$ m^2. The effective thermal conductivity of the liquid-saturated wick is calculated using the equation given in Dunn and Reay[5] for sintered wicks. The nucleation radius of the vapor bubbles r_n is taken as 2.54×10^{-7} m, which is given in Chi.[4] The results in Figs. 1–4 were obtained for a vapor temperature at $r = 0$ of 80°C. Unless otherwise noted, the default design parameters used for Figs. 1–4 are the values given previously.

Parameter Effects

The effects of the internal flow channel angle on the maximum heat transfer capacity is shown in Fig. 1. The parameter $Da = K/\varepsilon h^2$, is the modified Darcy number of the porous wick, which represents the effects of the wick structure. For any given horizontal and vertical wick structures there exists an optimum flow channel angle. The optimum value occurs due to the influence of the flow channel angle on both the vapor and liquid flows. A large flow channel angle results in

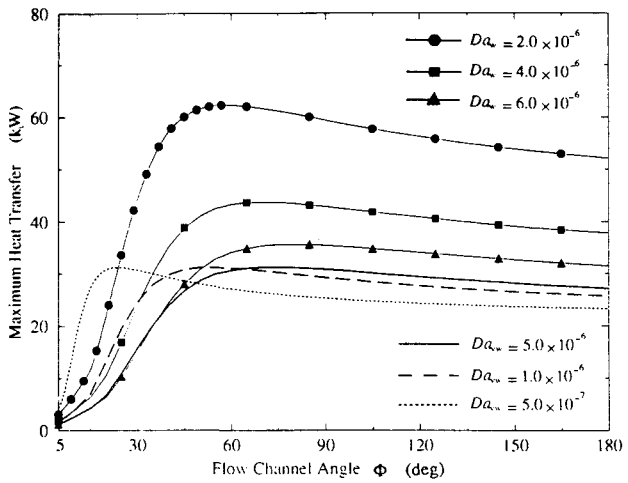

Fig. 1 Variations of maximum heat transfer as a function of the internal flow channel angle.

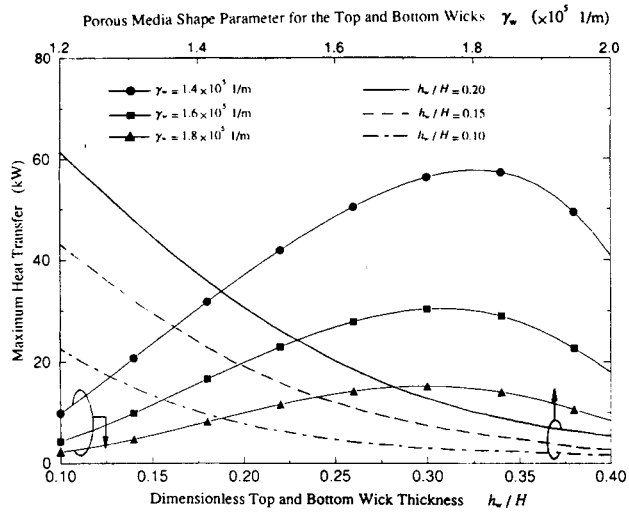

Fig. 2 Effects of the top and bottom wick structure on the maximum heat transfer.

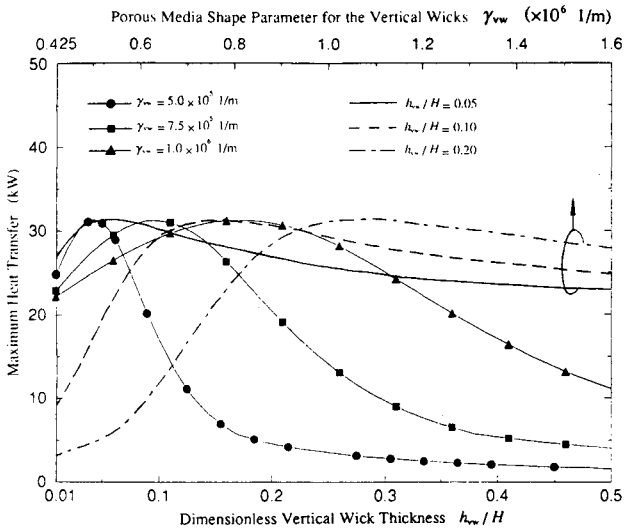

Fig. 3 Effects of the vertical wick structure on the maximum heat transfer.

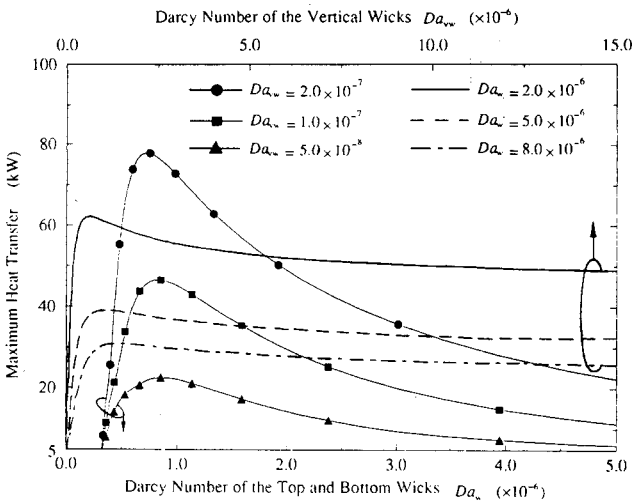

Fig. 4 Variations of maximum heat transfer as a function of Darcy numbers Da_w and Da_{vw}.

an increased vapor space and a decreased vapor flow resistance, thus increasing the maximum heat transfer capacity. Conversely, a large flow channel angle results in less vertical wicks, such that decreases the cross-sectional area of liquid flow from the bottom wick to the top wick, hence, decreasing the maximum heat transfer capacity. The balance of these two effects leads to an optimum flow channel angle. It can be seen in Fig. 1 that the optimum flow channel angle depends more strongly on the vertical wick structure than on the top and bottom wick structure. However, the optimum maximum heat transfer depends mostly on the top and bottom wick structure.

The effects of top and bottom wick structure on the maximum heat transfer capacity is illustrated in Fig. 2. Increasing the top and bottom wick thickness results in a decreased resistance to liquid flow within the top and bottom wicks, hence, increasing the maximum heat transfer capacity. In addition, for a fixed total thickness of the heat pipe $H = h_v + 2h_w$, increasing the top and bottom wick thickness leads to a decreased capillary rise height of the vertical wicks, thus decreasing the resistance to the liquid flow from the bottom wick to the top wick through the vertical wicks. However, increasing the top and bottom wick thickness results in a decreased vapor space thickness, thus increasing the resistance to the vapor flow. The balance between the decreased

liquid resistance in both horizontal and vertical wicks and the increased vapor resistance leads to an optimum top and bottom wick thickness, as shown in Fig. 2. Figure 2 also shows that the maximum heat transfer decreases monotonically with increasing the top and bottom wick shape parameter $\gamma_w = \sqrt{\varepsilon_w/K_w}$. Based on the investigation of flow through porous media by Vafai and Tien,[6] an increase of γ_w leads to a larger flow resistance in the wick, and thus, to a lower maximum heat transfer.

Figure 3 shows the effects of vertical wick structure on the maximum heat transfer capacity. An optimum vertical wick thickness exists for any given porous media shape parameter of the vertical wick $\gamma_{vw} = \sqrt{\varepsilon_{vw}/K_{vw}}$. A large vertical wick thickness leads to a large flow rate of liquid from the bottom wick to the top wick, and thus, to a higher maximum heat transfer. On the other hand, a large vertical wick thickness produces a larger resistance to the vapor flow due to the decrease of the vapor space, thus decreasing the maximum heat transfer. The balance of these two effects leads to an optimum vertical wick thickness for the maximum heat transfer capacity. Figure 3 also shows that for any given vertical wick thickness an optimum vertical wick shape parameter is observed. The optimum value occurs due to the influence of the vertical wick material on both the frictional resistance to the liquid flow within the vertical wicks and the capillary force of the vertical wicks. A large vertical wick shape parameter increases the frictional resistance to the liquid flow in the vertical wicks, thus decreasing the flow rate of liquid from the bottom wick to the top wick. Conversely, a large vertical wick shape parameter increases the capillary force of the vertical wicks, thus increasing the liquid flow rate in the vertical wicks. The internal balance of these two effects leads to the optimum vertical wick shape parameter.

Optimization of the Heat Pipe Design

To simplify the optimization of the disk-shaped heat pipe design, the Darcy number is used to reflect the effects of the wick structure (both the wick thickness and the porous wick shape parameter), as shown in Fig. 4. Therefore, the maximum heat transfer capacity of the disk-shaped heat pipe is a function of the internal flow channel angle, the Darcy number of the top and bottom wicks, and the Darcy number of the vertical wick. Figures 1 and 4 are then used to optimize the disk-shaped heat pipe design.

It should be mentioned that the use of Fig. 4 requires a judicious use of the parameters. As shown in Fig. 4, an optimum Da_w exists for the heat pipe design. Different wick material and thickness can be selected to obtain this optimum value of Da_w. Since $Da_w = 1/(\gamma_w h_w)^2$, and the maximum heat transfer capacity increases dramatically as γ_w decreases, it is preferred to select a smaller γ_w and a larger h_w to obtain a better result. However, from the boiling limitation considerations, a smaller γ_w or a larger h_w results in an increased thermal resistance to the heat transfer across the liquid-saturated wick, thus decreasing the maximum vertical heat flux of the disk-shaped heat pipe. Therefore, the boiling limitation should be taken into consideration when selecting wick material and thickness.

Conclusions

A pseudo-three-dimensional analytical model has been formulated for the parametric study of the maximum heat transfer capacity of a disk-shaped heat pipe. The maximum heat transfer capacity was evaluated as a function of design parameters based on the capillary limitation. The results show that, for a fixed heat pipe thickness, the optimized flow channel angle, top and bottom wick thickness, vertical wick thickness, and shape parameter of the vertical wicks exist for which the capillary limit of the disk-shaped heat pipe reaches a maximum value. An optimized disk-shaped heat pipe design was obtained based on the parametric study and the boiling limitation.

Acknowledgments

This work was supported by the Department of Energy under Contract DE-FGO2-93ER61612. The authors would like to thank Thomas Blue for his help on this work.

References

[1]Vafai, K., Zhu, N., and Wang, W., "Analysis of Asymmetrical Disk-shaped and Flat Plate Heat Pipes," *Journal of Heat Transfer*, Vol. 117, No. 1, 1995, pp. 209–218.

[2]Zhu, N., and Vafai, K., "The Effects of Liquid-Vapor Coupling and Non-Darcian Transport on Asymmetrical Disk-Shaped Heat Pipes," *International Journal of Heat and Mass Transfer* (to be published).

[3]Vafai, K., "Convective Flow and Heat Transfer in Variable Porosity Media," *Journal of Fluid Mechanics*, Vol. 147, 1984, pp. 233–259.

[4]Chi, S. W., *Heat Pipe Theory and Practice*, Hemisphere, New York, 1976.

[5]Dunn, P. D., and Reay, D. A., *Heat Pipes*, 3rd ed., Pergamon, New York, 1982.

[6]Vafai, K., and Tien, C. L., "Boundary and Inertia Effects on Flow and Heat Transfer in Porous Media," *International Journal of Heat and Mass Transfer*, Vol. 24, No. 2, 1981, pp. 195–203.

Direct Least-Square Solutions to Integral Equations Containing Discrete Data

J. I. Frankel*
University of Tennessee, Knoxville, Tennessee 37996-2210

Introduction

MATHEMATICAL models in engineering and physics often contain noisy discrete data. Yet it is often desired to obtain a solution to either a differential or integral equation in the presence of such data. Shih et al.[1] encountered such a situation where an experiment was devised to map the intensity of thermal radiation leaving a diffuse hemispherical shell. Shih et al. developed a simplified mathematical model that was expressed in terms of a Fredholm integral equation of the second kind. Interestingly enough, this equation permits an exact solution. In this case, the radiosity distribution along the surface of the hemisphere is expressible in terms of an integral containing the surface temperature distribution raised to the fourth power.

Instrumental to the success of that study was the availability of the exact solution for the radiosity distribution. Unfortunately, most situations preclude the determination of the exact solution for an integral equation that is derived from radiative heat transfer. In response to this dilemma, this Note revisits the exposition of Shih et al. and presents a general method for determining the unknown radiosity in the presence of noisy discrete temperature data based solely on knowledge of the

Received April 26, 1995; revision received June 30, 1995; accepted for publication Aug. 10, 1995.

*Associate Professor, Mechanical and Aerospace Engineering Department. Member AIAA.